Available online at www.sciencedirect.com
SCIENCE DIRECT®
Journal of the European Ceramic Society 25 (2005) 2045–2049
www.elsevier.com/locate/jeurceramsoc

Density improvement of the sol–gel dip-coated SnO_2 films by chemical surface modification

A.P. Rizzato [a,b], C.V. Santilli [a], S.H. Pulcinelli [a], P. Hammer [a], V. Briois [b,*]

[a] *Institute of Chemistry, Unesp P.O. Box 355, Araraquara, SP, Brazil*
[b] *LURE-Centre Universitaire Paris-Sud, Bât 209D, P.O. Box 34, 91898 Orsay Cedex, France*

Available online 12 April 2005

Abstract

We compare the effect of organic (Tiron®) and inorganic (Mn(II)) additives on the low temperature (<600 °C) densification of the sol–gel dip-coated SnO_2 films. The structural and compositional properties of the samples were investigated by X-ray reflectometry (XRR), X-ray absorption spectroscopy (XAS) and X-ray photoelectron spectroscopy (XPS). The results suggest that the replacement of hydroxyl groups at the particle surface by Tiron® reduces the level of agglomeration of the sol, increasing the particles packing and the apparent density of the coatings. Undoped and Mn-doped films drawn from a Tiron® containing suspension show after firing at 500 °C a porosity reduction of 12 and 8.6%, respectively. The porosity decrease is less pronounced (4.3%) for the film without additives. Both XAS and XPS data show the presence of trivalent manganese. The formation of a non-homogeneous solid solution characterised by the presence of Mn(III) replacing tin atom near to the crystallite surface was evidenced by XAS. Additionally, XPS results reveal the presence of metallic Sn at the surface of films containing Tiron®.

Keywords: Sol–gel processes; Films; Firing; Porosity; X-ray methods

1. Introduction

Tin oxide films are well known for their unique combination of properties such as high electrical conductivity, high transparency in the visible spectral range, thermal stability, and chemical corrosion resistance.[1] These characteristics make it a material of choice for a number of applications like antistatic coatings,[2] electrodes for flat panel display,[1] and transparent corrosion resistant coatings.[1] To satisfy the requirements of this wide field of applications, a growing effort has been made to synthesise SnO_2 films by using the sol–gel process.[2] However, due to the high porosity of the as-prepared films (up to 50%), post-firing steps are indispensable to achieve the desired combination of properties. The difficulty to prepare dense SnO_2 ceramics is well known and the use of the sintering additives such as Cu(II) or Mn(II) have shown to be very effective in the densification upon firing at temperatures above 900 °C.[3,4] However, this temperature range is incompatible with the classical glass coating technology. Furthermore, controversies already exist to explain the sintering process of doped SnO_2 ceramics with different hypotheses: lattice diffusion, liquid-state diffusion, demixing, and fast redistribution of solute.[3,4]

The objective of this work is two-fold: first, to test a new approach that can provide a high density of as-deposited sol–gel films, limit the grain growth and improve the densification upon low firing temperature (<600 °C). The basic principle of this approach is based on the modification of surface properties of SnO_2 nanoparticles by the replacement of surface hydroxyl groups by small ionic molecules that hinders the colloidal aggregation, does not condense as OH does, and could eventually pin the grain boundaries. We test these ideas by using Tiron® capping molecules, recently reported as SnO_2 nanoparticles dispersant and crystallite growth controller,[5] combined with addition of manganese as a sintering additive. The second goal is to obtain more information about the role of these additives on the sintering

* Corresponding author. Tel.: +33 1 64 46 80 20; fax: +33 1 64 46 41 48.
E-mail address: briois@lure.u-psud.fr (V. Briois).

0955-2219/$ – see front matter © 2005 Elsevier Ltd. All rights reserved.
doi:10.1016/j.jeurceramsoc.2005.03.009

mechanism of SnO_2 films. For this purpose, the density and thickness of the films were determined by X-ray reflectometry (XRR), the local order around Sn and Mn studied by X-ray absorption spectroscopy (EXAFS and XANES) and the film composition and bonding structure were determined by X-ray photoelectron spectroscopy (XPS).

2. Experimental

As previously described, a transparent and stable SnO_2 colloidal suspension was prepared by the hydrolysis of $SnCl_4{\cdot}5H_2O$ in aqueous solution promoted by the addition of a concentrated ammonium hydroxide solution.[6] In the case of Mn-doping and Tiron® (4,5-dihydroxy,1,3-benzene disulfonic acid, disodium salt, $((OH)_2C_6H_2(SO_3Na)_2)$) grafted nanoparticles, sols were prepared according Ref. [5]. A concentrated aqueous ammonia solution was added to a tin chloride ($SnCl_4{\cdot}5H_2O$) aqueous solution (0.63 mol L^{-1}, pH < 1) containing 10 wt.% of Tiron® and 3 wt.% of manganese ($MnCl_2{\cdot}4H_2O$) with respect to SnO_2. The precipitate kept in the mother solution was heated under reflux at 100 °C during 90 min. Then, the chemically modified and doped powder was isolated by centrifugation at 14 000 rpm during 15 min and washed with bi-distilled water. This step was repeated several times in order to eliminate the remaining ions of the reaction (mainly chloride and sodium). The isolated powder was dried at 80 °C for 12 h and then redispersed in concentrated tetrapropylammonium hydroxide (TPAH) aqueous solution at pH 11 under ultrasonic vibration (20 kHz). The films were deposited by dip-coating (drawn speed of 8 cm min^{-1}) from the prepared colloidal suspension on cleaned Corning 7059 glass slides. After drying at 100 °C, the films were treated for 30 min at 300, 400 and 500 °C.

XRR curves were measured with a powder diffractometer (D5000, Siemens) using monochromatic Cu Kα radiation (1.5418 Å). The accuracy in incident and detection angles was 0.001° and the width of both entrance and receiving slits were 0.01 mm to minimize angular divergence. The simulation of experimental reflectivity curves was performed using the Refsim® software (Siemens), which is based on the formalism developed by Nèvot and Croce.[7] The resulting agreement factor was $R < 0.8$ and the accuracy for density and thickness about ±7% and ±0.5 nm, respectively.[8] The XAS measurements were carried out at the D44 station of the LURE synchrotron source (Orsay, France). Sn K-edge spectra (29.2 keV) were recorded in transmission mode at room temperature over 1200 eV with 4 eV energy steps using a Ge(4 0 0) double crystal monochromator (DCM). Mn K-edge EXAFS (resp. XANES) spectra were measured in fluorescence mode using a solid-state Si(Li) seven-elements detector and using a Ge(1 1 1) (resp. Si(1 1 1)) DCM detuned by a factor of 40% to suppress higher order harmonics. Mn K-edge EXAFS data were recorded over 550 eV with 2 eV of energy step and 5 s of counting time, whereas XANES data were obtained over 120 eV with 0.3 eV of energy step. The software package *Round Midnight*[9] was used to fit the weighted $k^n\chi(k)$ EXAFS spectra, with input from crystallographic data of reference samples. Ab initio calculations at the Mn K-edge were done by using the FeFF7 code in a similar way that those reported for Cu-doped SnO_2 xerogels.[3] The XPS analysis was carried out with an Omicron spectrometer, using the Al Kα line ($h\nu$ = 1486.6 eV; width, 0.85 eV) and the analyser pass energy was set to 10 eV. The elastic background of the Sn 3d, O 1s, Mn 3d and C 1s electron core-level spectra was subtracted and the composition was determined from the ratio of the relative peak areas corrected by sensitivity factors of the corresponding elements. All spectral components were fitted by a multiple peak Voigt profile without placing constraints. The width at half maximum varied between 1.6 and 1.9 eV and the accuracy of the peak positions was ±0.1 eV.

3. Results and discussion

Fig. 1 displays the evolution of X-ray reflectivity curves upon firing of SnO_2 films prepared from colloidal suspensions without additives, containing Tiron® and with a combination of Tiron® and Mn-doping. The critical angles of total reflection, θ_c, of films prepared from sol containing Tiron® and manganese is larger that those corresponding to the films without additives. This result indicates that the apparent density is largest for films containing a combination of Tiron® and manganese additives. A plausible explanation for this finding is the increase of particle packing due to expected reduction of colloidal aggregation of Tiron® grafted samples. Furthermore, the observation of the θ_c increase with temperature for all samples proves the densification effect induced by the post-annealing process. The fitted values of

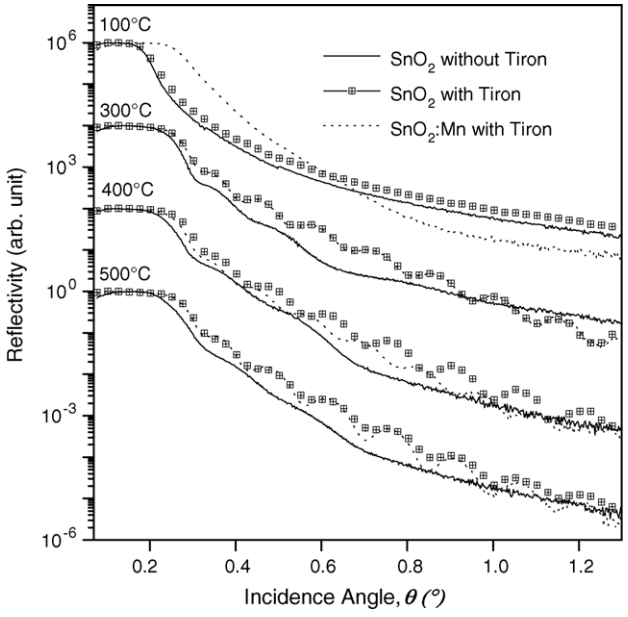

Fig. 1. X-ray reflectivity curves of tin oxide thin films dip-coated from three different colloidal suspensions fired at 100, 300, 400 and 500 °C.

Table 1
Apparent density, porosity, thickness and tin atom coordination numbers determined from fitting of the X-ray reflectivity curves and EXAFS Sn K-edge spectra of films treated at different temperatures

Temperature (°C)	Density (g/cm^3)			Porosity (%)			Thickness (nm)			Coordination numbers								
										N_0 (Sn—O)			N_1 (Sn—Sn)			N_2 (Sn—Sn)		
100	3.2	3.5	3.8	54.3	50.0	45.7	–	–	–	5.9	5.7	–	1.5	1.7	–	5.0	4.8	–
300	3.3	3.9	4.1	52.8	44.3	41.4	26	29.6	30	6.0	5.5	5.1	1.6	1.5	1.5	5.6	5.3	5.9
400	3.3	3.8	4.3	52.8	25.7	38.6	25	30.7	27.9	5.7	5.5	5.5	1.5	1.9	2.0	7.5	6.8	6.4
500	3.5	4.3	4.4	50	38.6	37.1	21.8	27.8	27.8	5.9	5.8	6.0	1.3	1.9	2.0	8.0	7.9	6.7

For each item, the first, second and third column is related to undoped SnO_2, Tiron® modified SnO_2 and to manganese doping chemically modified SnO_2 films, respectively. Typical accuracies for the EXAFS coordination numbers are 10% for N_0 and 20% for N_1 and N_2.

apparent density and thickness are summarised in Table 1. The fact that all densities are lower than that of SnO_2 cassiterite single crystal ($\rho = 7.0\,g\,cm^{-3}$) shows that the films are quite porous. The porosity was calculated from the apparent density (ρ_a) using the relation, $P = 1 - \rho_a/\rho$. The treatment at 500 °C leads to about 12 and 8.6% porosity decrease for the undoped and Mn-doped films drawn from a Tiron® containing suspension, respectively. In contrast, at the same conditions the SnO_2 films prepared without additives showed a porosity reduction of 4.3%.

The Fourier transforms (FT) of the Sn K-edge EXAFS spectra of films grown from the different suspensions are shown for different annealing temperatures in Fig. 2. For all FT the first peak at ∼1.6 Å, labelled 1, is related to the first coordination shell of oxygen atoms located at 2.06 Å. The second peak, labelled 2, displays two components at ∼2.8 and 3.4 Å due to the first and second tin coordination shell located at 3.20 and 3.72 Å, respectively.[3] These distances,

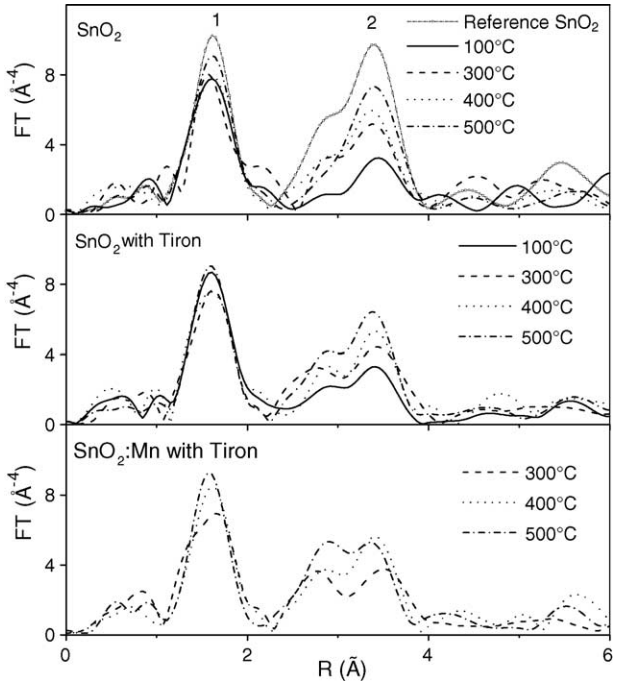

Fig. 2. Fourier transforms of the EXAFS spectra recorded at the Sn K-edge for the films fired at different temperatures deposited from three different colloidal suspensions.

determined by least-square fitting procedure, are almost independent on the suspension preparation route, indicating a cassiterite like-structure. The firing of nanoparticles usually leads to an increase of the intensity of EXAFS peaks related to the cation–cation contributions. This is due to two concomitant effects: the decrease of the disorder, which is related to the pseudo Debye–Waller factor, and the crystallite growth that leads to an increase of the mean cation coordination number.[3] The relation between the EXAFS coordination number for nanoparticles and their average grain size is well known. For isotropic SnO_2 nanoparticles, this relation has been established by Serrini et al.[10] We note here that the intensity increase of the second peak with temperature is less pronounced for Tiron® containing samples. For the same firing temperature, the pseudo Debye–Waller factors determined by a fitting procedure have been found of the same order of magnitude for the different samples. It indicates that the differences in peak intensity for samples fired at the same temperature are mainly due to the changes in the coordination number.

Up to 400 °C, the average number of second tin neighbouring atoms (N_2) (Table 1) is lower for films prepared with Tiron® than the number for films prepared without Tiron®. This suggests that the Tiron® layer covering the crystallite surface inhibits a significant particle growth at low temperatures. The thermal decomposition of Tiron® occurs around 400 °C.[5] We observe concomitantly a crystallite growth evidenced by the increase of N_2. It is interesting to compare the shape of peak 2 for the different films at each firing temperature. This peak for the chemically modified films always displays a shape rather similar to the shape of the second peak measured on a bulk crystalline SnO_2 reference, whereas for films prepared without Tiron®, the prominent shoulder at 2.8 Å almost disappears above 300 °C. On one hand, this behaviour indicates an isotropic growth of the SnO_2 nanocrystallite for the chemically modified films, which exists even after the fragmentation of Tiron® molecules. On other hand, this evidences a preferential particle growth for the films prepared without Tiron® at 500 °C. Such preferential growth was attributed to diffusion anisotropy characteristic of cassiterite structure that plays an important role on the pores growth due to grains coalescence.[11] The crystallite size growth upon firing revealed by the increase of N_2 (Table 1) was confirmed by X-ray diffraction measurements. For instance, the average

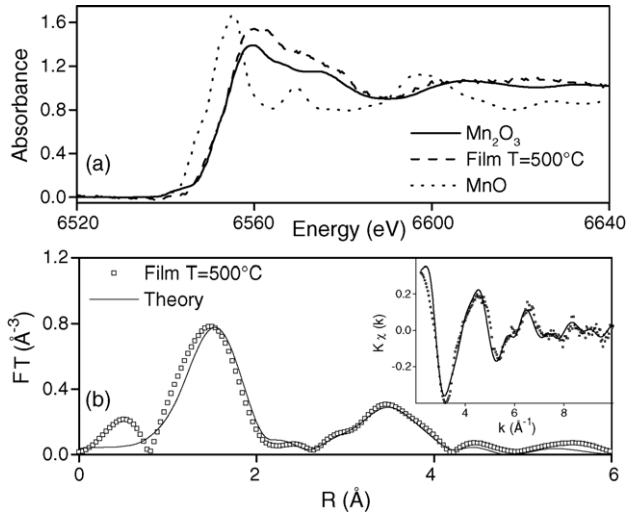

Fig. 3. (a) XANES spectrum recorded for the film fired at 500 °C compared to MnO and Mn_2O_3 used as a manganese divalent and trivalent references, respectively. The edge position is clearly in coincidence with the edge position of the trivalent reference. (b) Fourier transform of the EXAFS spectrum (dot line) recorded at the Mn K-edge for the film doped with Mn and chemically modified with Tiron® fired at 500 °C. Theoretical Fourier transform (full line) of the EXAFS spectrum for manganese into a substitutional site for into an idealised crystallite SnO_2. The theoretical and experimental EXAFS spectra are compared in the inset.

crystallite size increases from 77 to 90 Å as the firing temperature increases from 400 to 500 °C for Tiron® free SnO_2 and from 57 to 78 Å for Tiron® SnO_2 containing films. Finally it is noteworthy that the N_2 values of the manganese-doped films fired at 400 and 500 °C is smaller than the N_2 of the undoped films (Table 1). This indicates that the manganese doping inhibits the crystallite growth, which can be due to a reduction of the grain boundary mobility.

Mn K-edge XANES results presented in Fig. 3(a) clearly evidences the trivalent oxidation state for manganese in the doped films. The manganese distribution into the SnO_2 matrix has been determined by EXAFS measurements at the Mn K-edge. Upon heating no remarkable modification of the local order around manganese is observed, then only the FT of the manganese-doped film fired at 500 °C is reported in Fig. 3(b). The first peak located at 1.5 Å can be satisfactorily reproduced using a coordination shell of 3.8 ± 0.5 oxygen atoms at 1.97 ± 0.02 Å. This distance is in agreement with Mn–O distance found for trivalent manganese. In that case, the ionic radius of doping is faintly smaller than to the radius of Sn(IV) and the formation of Mn(III) solid solution can be then envisaged. This has been fully confirmed with ab initio EXAFS calculations, presented in Fig. 3(b) and in the inset, where spectra were simulated considering that a manganese atom replaces a tin atom present at the surface site of an idealised SnO_2 crystallite. Details on the calculations and of the site position (site e) in the idealised structure can be found in Ref. [3]. These results evidence the formation of a substitutional solid solution between SnO_2 and Mn(III) introducing oxygen vacancies in the cassiterite lattice. The lattice diffusion can be consequently improved favouring the low-temperature densification.

The compositional analysis of the XPS data shows that all films are oxygen deficient with $[O]/[Sn] = 1.8 \pm 0.2$ and contain carbon bonds. The determined manganese concentration of 2.8 ± 0.4 wt.% is in good agreement with the nominal value of 3 wt.%. The noisy Mn $2p_{3/2}$ spectrum (not shown) presents a main component at 641.5 eV indicative for Mn(III) species like in Mn_2O_3 structures. This result totally confirms the oxidation state of manganese found by Mn K-edge XANES results.

The deconvoluted O 1s and Sn $3d_{5/2}$ core-level spectra of the Tiron® and manganese containing samples treated at 100

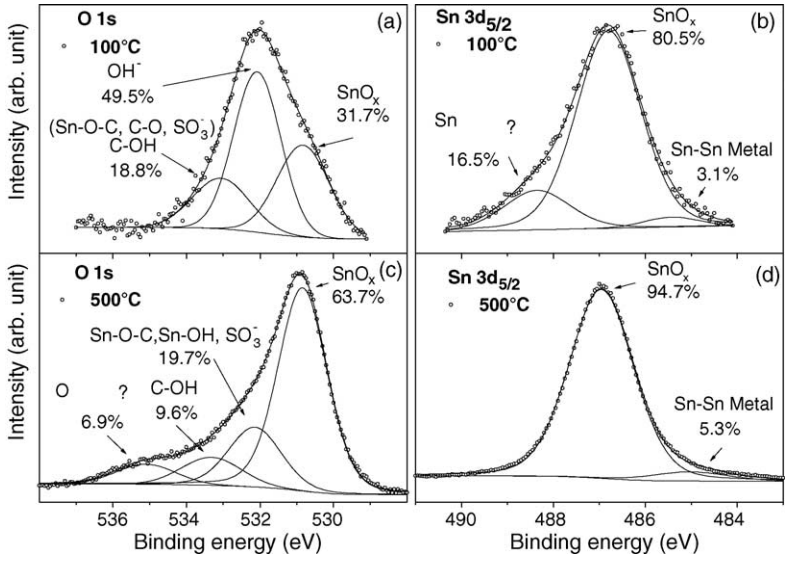

Fig. 4. Fitted XPS O 1s and Sn $3d_{5/2}$ spectra of the manganese-doped Tiron® containing SnO_2 films dried at 100 °C (a) and (c) and fired at 500 °C (b) and (d), respectively.

and 500 °C are displayed in Fig. 4(a and c) and (b and d), respectively. As expected, the most prominent component of the O 1s spectrum at 530.7 eV, for the film treated at 500 °C, reveals the dominance of tin oxide bonds. The sub-peak at 532.1 eV is attributed to Sn–O–C and SO_3^- bonds related to Tiron® derivatives and a small quantity of terminal Sn–OH bonds.[12] The sub-peak at 533.3 eV is assigned to adsorbed C–OH groups on the film surface. The origin of the small contribution at 535.2 eV spectrum side is not clear, but one possible attribution is oxygen bonded to the aromatic ring of the Tiron® molecule. In contrast, the sample dried at 100 °C shows a main component of the O 1s spectrum at 532.1 eV and a sub-peak at 533.2 eV related mostly to adsorb OH^- and C–OH groups, respectively.[12] The presence of a contamination layer is evidenced by the intense component of adventitious carbon observed in the C 1s peak at 284.8 eV (not shown). The fact that for the film treated at 500 °C only an insignificant surface contamination was detected, can be explained by the temperature driven desorption of atmospheric species.

The main contribution to the Sn $3d_{5/2}$ peak intensity at 487.0 eV of samples treated at 100 and 500 °C comes from the presence of the tin-oxide species, detected in the O 1s spectra (Fig. 4(b and d)). The small component found at lower binding energy (485.0 eV) is attributed to a small fraction of metallic tin phase. The percentage of the peak increases with temperature from 3.1 ± 0.2 to 5.3 ± 0.3%. The existence of a metallic phase was detected also in XPS spectra of undoped Tiron® containing samples but with a smaller concentration (typically around 3.0% after firing at 500 °C). For samples free of Tiron® and manganese, the XPS analysis does not reveal the presence of such Sn metallic phase. This finding hints at a possible SnO_2 reduction induced by Tiron® and manganese oxidation. The heat released by the organic combustion could also induce the superficial evaporation of SnO_2 and the condensation of metallic Sn phase.

4. Conclusions

XRR and EXAFS data show that the surface modification of SnO_2 particles by Tiron® molecule improves the particle packing, increasing the apparent density of as-dried films. The presence of Tiron® molecules grafted to the surface of particles inhibits the crystallite growth during moderate temperature firing ($T \leq 400$ °C). Further film densification can be achieved by addition of manganese. The oxidation of Mn(II) into Mn(III) have been shown both by XANES and XPS. This favours the formation of a non-homogeneous solid solution in which Mn(III) replaces Sn(IV) lattice position near the surface of crystallite. The inhibition of the crystallite growth by Tiron® grafting together with the improvement of the lattice diffusion due to the formation of the Mn_{Sn}–SnO_2 solid solution contribute to the densification of films at low firing temperature. Finally, the XPS results reveal the presence of a small fraction of metallic Sn–Sn bonds attributed to the oxy-reduction reactions during combustion of Tiron® molecules and the change of oxidation state of manganese.

Acknowledgements

This work has been supported by CAPES, CAPES-/COFECUB, FAPESP and CNPq.

References

1. Blunden, S. J., Cusack, P. A. and Hill, R., *The Industrial Uses of Tin Chemicals*. Royal Soc. Chem., London, 1985 [chapters 9 and 10].
2. Uhlmann, D. R., Suratwala, T., Davidson, K., Boulton, J. M. and Teowee, G., Sol–gel derived coatings on glass. *J. Non-Cryst. Solids*, 1997, **218**, 113–122.
3. Santilli, C. V., Pulcinelli, S. H., Brito, G. E. S. and Briois, V., Sintering and crystallite growth of nanocrystalline copper doped tin oxide. *J. Phys. Chem. B*, 1999, **103**, 2660–2667.
4. Gouvea, D., Smith, A., Bonnet, J. P. and Varela, J. A., Densification and coarsening of SnO_2-based materials containing manganese oxide. *J. Eur. Ceram. Soc.*, 1998, **18**, 345–351.
5. Santos, L. R. B., Chartier, T., Pagnoux, C., Baumard, J. F., Santilli, C. V., Pulcinelli, S. H. *et al.*, Tin oxide nanoparticles formation using a surface modifying agent. *J. Eur. Ceram. Soc.*, 2004, **24**, 3713–3721.
6. Hiratsuka, R. S., Pulcinelli, S. H. and Santilli, C. V., Formation of SnO_2 gels from dispersed sols in aqueous colloidal solutions. *J. Non-Cryst. Solids*, 1990, **121**, 76–83.
7. Nèvot, L. and Croce, P., Characterization of surfaces by grazing X-ray reflection—application to study of polishing of some silicate-glasses. *Rev. Phys. Appl.*, 1980, **15**, 761–779.
8. Grimal, J. M., Chartier, P. and Lehuédé, P., X-ray reflectivity: a new tool for the study of glass surfaces. *J. Non-Cryst. Solids*, 1996, **196**, 128–133.
9. Michalowicz, A., Round Midnight, EXAFS signal treatment and refinement programs, LURE, Orsay, France. Programs available on LURE website; http://www.LURE.fr.
10. Serrini, P., Briois, V., Horrillo, M. C., Traverse, A. and Manes, L., Chemical composition and crystalline structure of SnO_2 thin films used as gas sensors. *Thin Solid Films*, 1997, **304**, 113–122.
11. Brito, G. E. S., Santilli, C. V. and Pulcinelli, S. H., Anisotropy of crystallite growth during sintering of SnO_2 xerogels. *J. Mater. Sci.*, 1996, **31**, 4087–4092.
12. Wagner, C. D., Naumkin, A. V., Kraut-Vass, A., Allison, J. W., Powell, C. J. and Rumble Jr, J. R., NIST standard reference database 20, version 3.4, web version: http://srdata.nist.gov/xps.